KeAi
CHINESE ROOTS
GLOBAL IMPACT

#### Contents lists available at ScienceDirect

# Petroleum Science

journal homepage: www.keaipublishing.com/en/journals/petroleum-science



# Original Paper

# Acoustic logging response law in shales based on petrophysical model

Song Hu  $^{\rm a,\,*}$ , Wei-Nan Liu  $^{\rm b}$ , Ying-Ming Liu  $^{\rm c}$ , Kun Liu  $^{\rm a}$ 



- <sup>a</sup> Petroleum Exploration and Production Research Institute, SINOPEC, Beijing, 100083, China
- <sup>b</sup> Shenzhen Branch of CNOOC (China) Co., Ltd., Shenzhen, Guangdong, 518067, China
- <sup>c</sup> Research Institute of Petroleum Exploration and Development, CNPC, Beijing, 100083, China

# ARTICLE INFO

Article history: Received 1 March 2021 Accepted 12 January 2022 Available online 17 March 2022

Edited by Jie Hao

Keywords:
Shale reservoir
Acoustic logging
Response law
Complex pore structure
Clay
Fracture
Organic matter

#### ABSTRACT

Shale acoustic logging response law is complex due to the multiple minerals and pores, which limits the application of acoustic logging in shale reservoir parameter evaluation, therefore clarifying the shale acoustic logging response law is of great importance. Different petrophysical models are adopted for the equivalence of organic matter, clay, matrix minerals, and fractures, in Wufeng-Longmaxi shale formation in the Jiaoshiba area. Finally, the self-consistent approximation model is used to combine different components, and a shale petrophysical model with a complex pore structure is constructed. The model verification results show it has good predictability for shale. Based on the model, the effect of different mineral compositions and different types of pores are studied. The results show that: 1) The effect of clay and organic matter is very complex, and the variation laws of layered clay (organic matter) and dispersed clay (organic matter) on the acoustic wave are consistent. 2) Layered clay or organic matter leads to the formation anisotropy increase, which makes the acoustic time difference greater than that of containing dispersed clay (organic matter). 3) The fracture is the main control factor of anisotropy, and the anisotropy of gas-bearing fracture is higher than that of water/oil fracture.

© 2022 The Authors. Publishing services by Elsevier B.V. on behalf of KeAi Communications Co. Ltd. This is an open access article under the CC BY-NC-ND license (http://creativecommons.org/licenses/by-nc-nd/4.0/).

#### 1. Introduction

Shale oil and gas are important unconventional resources in the world. Due to the multiple influences of shale minerals and pores, the shale acoustic logging response law (ALRL) is complex, which brings difficulties to calculate the reservoir porosity, in-situ stress and other parameters and the fracturing ability evaluation, and makes logging evaluation divergent enhanced (Wang, 2015; Jin et al., 2016; Wu et al., 2016). Therefore, to provide valuable reference data and models for parameter evaluation, it is necessary to clarify the ALRL of different parameters before using acoustic data for shale evaluation.

The petrophysical model (PM) is an important method to study the ALRL. Many scholars have carried out theoretical research on PMs, which are mainly divided into equivalent medium theoretical model and pore elasticity theoretical model. Based on the equivalent medium theoretical model, Hill (1952) proposed the boundary theory model, Kuster and Toksöz proposed two-phase media with low porosity model (Kuster and Toksöz, 1974). Cleary (Clearry et al.,

\* Corresponding author.

E-mail address: husong.syky@sinopec.com (S. Hu).

1980) established the differential effective medium model (DEM) of the two-phase medium. Berryman established the self-consistent approximation (SCA) model in order to consider the influence of pore shape (Berryman, 1995). Based on the PE theory, Gassmann (Gassmann et al., 1951) constructed the relationship between elastic modulus and velocity of P-wave and S-wave in saturated rock. But the above PMs are based on the theory of isotropic equivalent medium, and they don't consider anisotropy.

In order to study the petrophysical laws of anisotropic reservoirs, different PMs can be combined. Combining the SCA model with the DEM model can calculate the effective elastic modulus of anisotropy shale (Hornby et al., 1994). Using the Gassmann model and Backus average model (Backus, 1962), can characterize the microscopic pore structure of organic-rich shale (Vernik et al., 2011). The SCA model and Backus average model combination can study the relationship between minerals, pores, rock mechanical parameters, and seismic response (Guo et al., 2013). Some models combine the DEM and Brown-Korringa fluid replacement model (Hu et al., 2014), or integrate Kuster-Toksöz model, SCA model, dual connected pore model, and linear sliding model to study the petrophysical response (Wang et al., 2019). But these PMs are mainly based on the theory of seismic petrophysical theory,

which is mainly used to study the relationship between seismic elastic properties (Ding et al., 2021; He et al., 2021) and reservoir characteristics (Aleardi, 2018; Wu et al., 2017; Qian et al., 2021). However, there are little researches on shale PMs and shale ALRL under high-frequency acoustic logging. At the same time, due to the differences in sedimentary environment, diagenesis, and thermal evolution degree of shale reservoirs in different regions, the petrophysical characteristics of different regions are different, and the PMs cannot be directly used. Taking the Jiaoshiba area in Sichuan Basin as an example, this paper constructs a high-frequency shale geophysical model suitable for complex pore structures base on the geophysics theory. Then, the acoustic response of different mineral compositions and different types of pores are studied by the model.

#### 2. Composition and pore structure

#### 2.1. Petrological characteristics

The experimental results of X-ray diffraction analysis of whole-rock minerals and clay minerals of 97 samples from Wufeng-Longmaxi formation in the Jiaoshiba area are shown in Fig. 1.

According to the analysis results, shale mineral components mainly include clay minerals, quartz, feldspar, calcite, and dolomite. Among them, the average contents of clay minerals, quartz, feldspar and carbonate rocks (calcite + dolomite) are 38.26% (11.8%–68.1%), 38.83% (10.3%–73.8%), 9.62% (2.2%–19.4%) and 12.68% (1.7%–74.7%) respectively. From top to bottom, the content of clay minerals shows a decreasing trend, while the quartz minerals gradually increase (Fig. 1a); at the same time, clay minerals are mainly composed of illite, chlorite, and illite mixed layers (Fig. 1b).

#### 2.2. Microscopic pore structure characteristics

According to the scanning electron microscope (SEM) photos, combined with the previous research knowledge on the area, the pores of the Wufeng-Longmaxi Formation are mainly clay pores (CLP), clastic pores (CP), organic matter pores (OMP) and fracture pores (FP) (Li et al., 2014). Among them, OMP is distributed in mature—high mature organic matter and fractures are mainly

micro-fracture of tectogenetic, interleaf fractures, and so on, as well as filled or partially unfilled high-angle fractures (Fig. 2).

The results in Fig. 1 show that clay minerals are the main ones in Wufeng-Longmaxi Formation. The development degree of CLP is closely related to the number and types of clay minerals in shale. The more clay minerals, the more developed the CLP, and the stronger ability of shale to absorb natural gas (Chen et al., 2016); however, due to the higher degree of evolution of shale in the studied interval, most of the pores in the clay minerals are not developed, and only a few of them can see intergranular pores and intercrystalline pores (fractures) (Fig. 2a and b), the clastic particles are mainly siliceous and a small amount of feldspar, in which the CP is the main oil storage space during the oil generation period, and these crude oils can form asphalt in the later evolution process, thereby providing a good pore carrier for OMP (Zhao et al., 2017).

The main kerogen in the study area is type I, and the vitrinite reflectance  $R_0$  is 2.2%—3.13%, which is mainly in the over-mature evolutionary stage (Shen et al., 2016). According to the SEM photos (Fig. 2), it is found that other types of pores are lost due to compaction and cementation, or are filled by migrated solid organic matter, among them, OMP is widely developed (Fig. 2e). Observation of the sample showthat most of the OMP exists in the solid asphalt, and the solid asphalt is a short-distance migration of organic matter.

There are a lot of micro-fractures in the Wufeng-Longmaxi. The micro-fractures in this part are mainly interlaminar seams, and their material composition is mainly laminar pyrite, calcite, and silt. In addition to interlayer fractures, high-angle structural fractures are also developed, and filled with calcite veins (Li et al., 2014), and in which the interlayer fractures are also developed (Fig. 2f).

The above analysis shows that the existing PMs are difficult to fully describe the micro-pore structure characteristics of the study area. To better study the change ALRL of shale, it is necessary to build a PM that conforms to shale characteristics.

## 3. The shale petrophysical model

Through the analysis of the basic characteristics, the mineral composition is diverse, and the pore structure is complex,

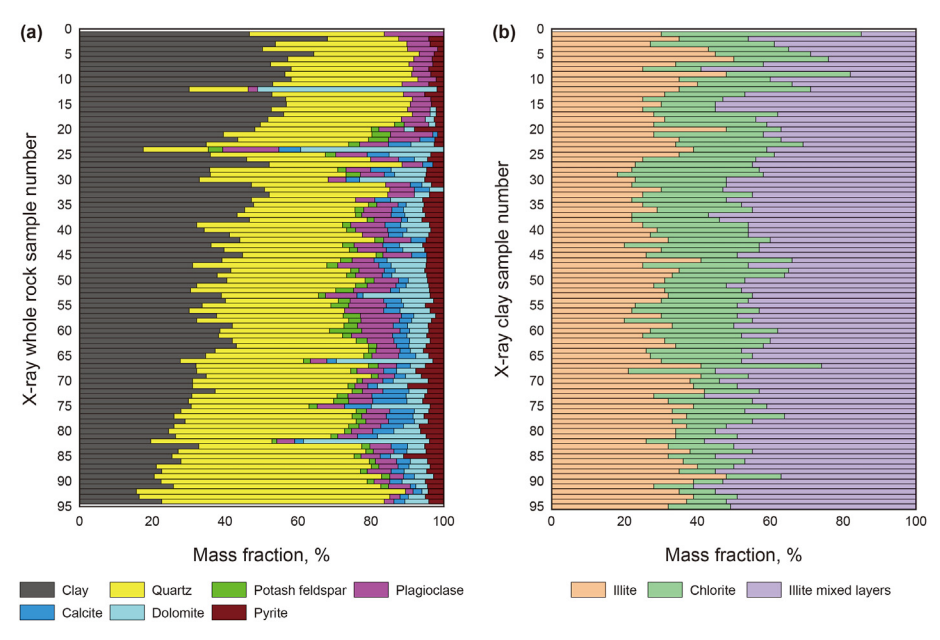


Fig. 1. Mineral distribution of Wufeng-Longmaxi in the study area.

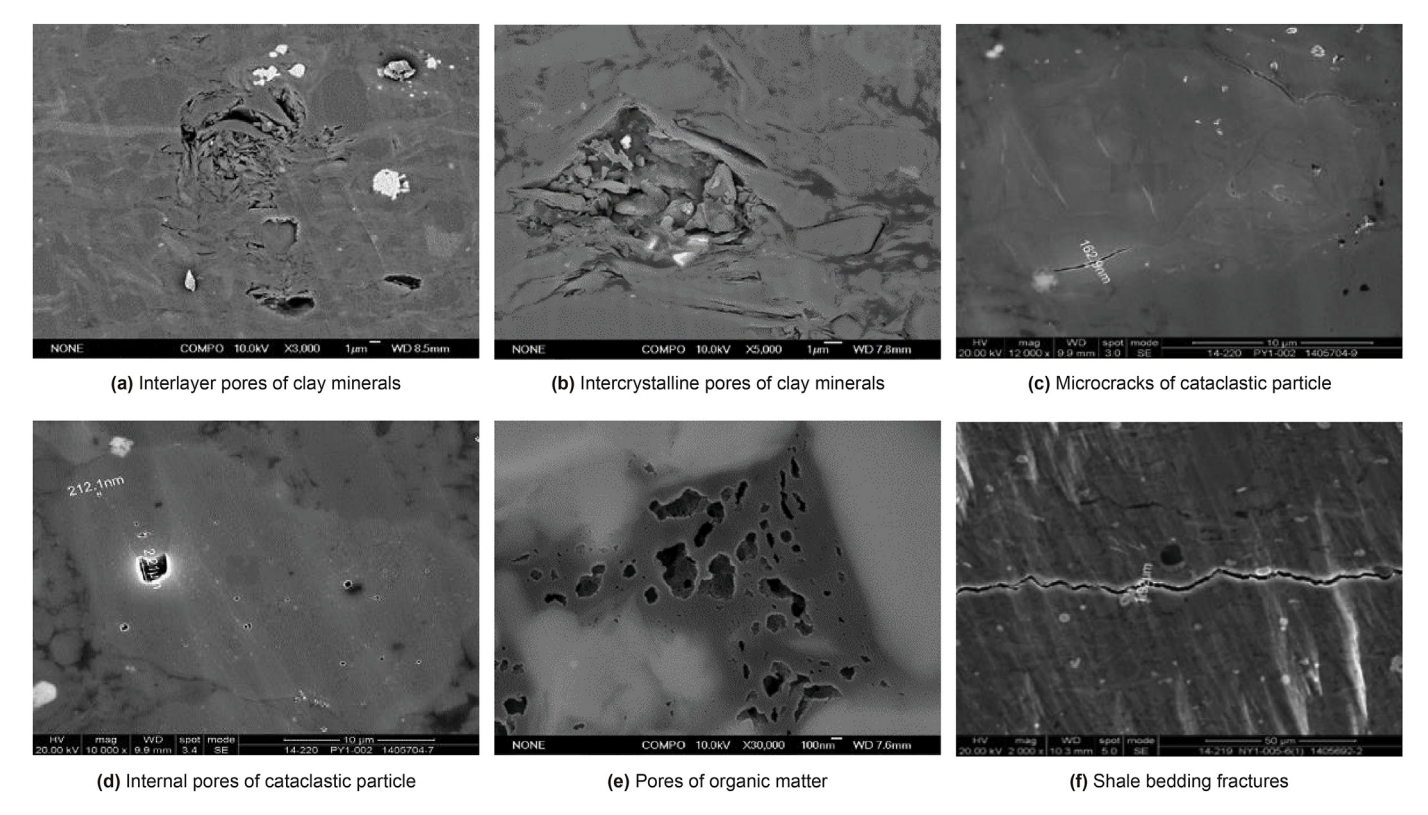


Fig. 2. SEM photos of micro pores and organic matter.

additionally the pore size is small. Given the special mineral and pore characteristics of shale, this paper uses the Kuster-Toksöz model, SCA model, Voigt equal strain average model, Backus model, linear sliding model, and Hudson model (Coates and Schoenberg, 1995; Hudson, 1981) to construct a shale PM suitable for ALRL. And the construction process is mainly divided into medium equivalent modulus calculation, anisotropic medium, and fracture fusion, and its flow chart is presented in Fig. 3.

#### 3.1. Calculation of equivalent elastic modulus

In this paper, first using the Kuster-Toksöz model to mix organic matter and organic matter pores to obtain mixed medium 1, second using the SCA model to mix clay minerals and clay pores to obtain mixed medium 2, then using the Voigt model to mix quartz and carbonate rocks to obtain mixed medium 3 (matrix minerals); and finally, the SCA model is used to mix these three media to obtain a shale rock model.

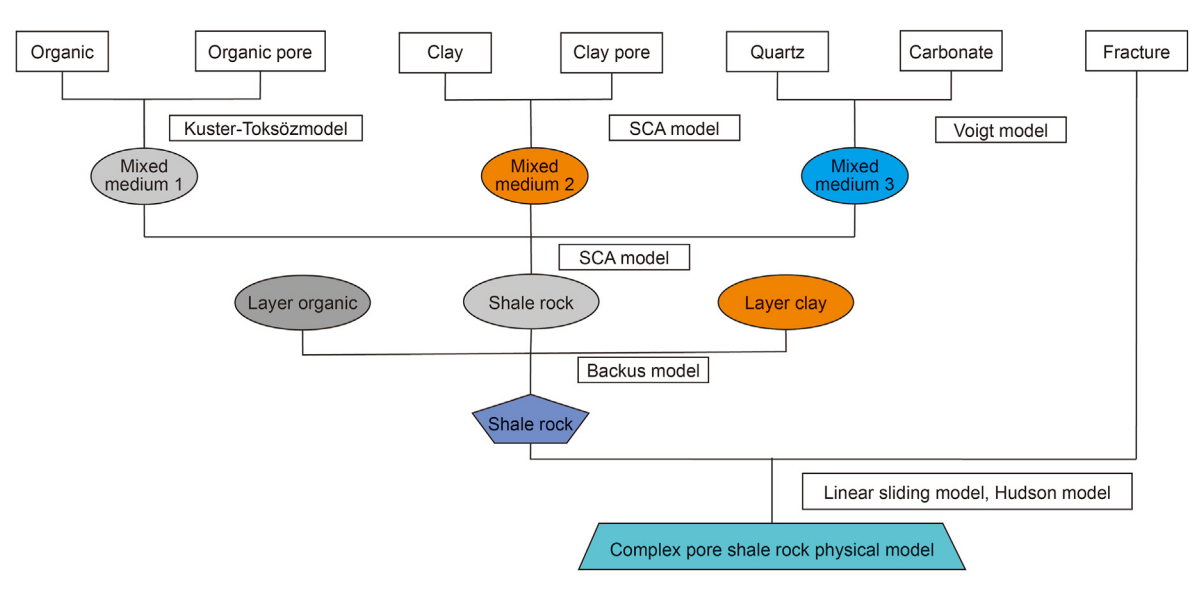


Fig. 3. Modeling flow chart of shale PM with complex pore structure.

#### 3.1.1. Equivalent modulus of organic matter

According to the core SEM photos, the organic matter is mainly distributed in block shape in shale, and the organic pores are mainly distributed in the organic matter in the shape of a circle or ellipse. Therefore, the dual-phase medium Kuster-Toksöz model, which is widely used and can characterize various pore shapes, is used to calculate the equivalent elastic modulus of the organic matter. The calculation formulas are shown in Eqs. (1) and (2) (Kuster and Toksöz, 1974).

$$\frac{K_{\text{ke}}}{K_{\text{k}}} = \frac{1 + \left[4\mu_{\text{k}}\left(K_{\text{f}} - K_{\text{k}}\right) / \left(3K_{\text{f}} + 4\mu_{\text{k}}\right)K_{\text{k}}\right]S}{1 - \left[3\left(K_{\text{f}} - K_{\text{k}}\right) / \left(3K_{\text{f}} + 4\mu_{\text{k}}\right)\right]S}$$
(1)

$$\frac{\mu_{ke}}{\mu_k} = \frac{(1-S)(9K_f + 8\mu_k)}{9K_k + 8\mu_k + S(6K_k + 12\mu_k)}$$
(2)

where, S is the fluid saturation, dimensionless;  $S = \Phi_f/(\Phi_f + \Phi_k)$ ,  $\Phi_f$  and  $\Phi_k$  are the volume of the fluid contained in the organic matter and the volume of the organic matter respectively, v/v;  $K_k$  and  $\mu_k$  are the bulk modulus and shear modulus of the organic matter respectively, MPa;  $K_{ke}$  and  $\mu_{ke}$  are the equivalent bulk modulus and shear modulus of organic matter containing fluid, MPa.

#### 3.1.2. Equivalent elastic modulus of clay

Considering the model is mainly applied to acoustic logging, and the clay pores in clay minerals are dominated by clay-bound water, the SCA model is used to calculate the equivalent bulk modulus (Eq. (3)) and shale modulus (Eq. (4)) (Berryman, 1995).

$$f_{\rm bw}(K_{\rm W} - K_{\rm c}^*)\beta^{\rm W} + f_{\rm c}(K_{\rm c} - K_{\rm c}^*)\beta^{\rm c} = 0$$
(3)

$$f_{\text{bw}}(\mu_{w} - \mu_{c}^{*})\zeta^{W} + f_{c}(\mu_{c} - \mu_{c}^{*})\zeta^{c} = 0$$
 (4)

where,  $K_{\rm W}$  and  $\mu_{\rm W}$  are the bulk modulus and shear modulus of water, MPa;  $K_{\rm C}$  and  $\mu_{\rm C}$  are the bulk modulus and shear modulus of clay, MPa;  $\beta$  and  $\zeta$  indicate the geometric factors of the content, the subscripts w and c, respectively represents water and clay;  $f_{\rm bw}$  and  $f_{\rm c}$  are the relative volumetric contents of clay bound water and clay, v/v, and  $f_{\rm bw}+f_{\rm C}=1$ .

#### 3.1.3. Equivalent elastic modulus of matrix mineral

Because there is little difference in strain between quartz and carbonate and other matrix minerals under the same conditions (Mavko et al., 2020). Therefore, the equal strain average model (Voigt model) is used to calculate the equivalent bulk modulus and shear modulus of the matrix mineral separate (Eq. (5)) (Hill, 1952).

$$K_{\text{me}} = \sum_{i=1}^{i=N} f_i K_i, \mu_{\text{me}} = \sum_{i=1}^{i=N} f_i \mu_i$$
 (5)

where,  $K_{\text{me}}$  and  $\mu_{\text{me}}$  are the equivalent bulk modulus and equivalent shear modulus of the matrix mineral, MPa;  $K_i$  and  $\mu_i$  are the bulk modulus and shear modulus of the i-th matrix mineral, MPa;  $f_i$  is the relative volume content of the i-th matrix mineral in the matrix part, v/v; N is the total type of matrix mineral.

#### 3.1.4. Calculation of overall equivalent modulus

The SCA model is utilized to calculate the equivalent bulk modulus and shear modulus of the whole model according to Eqs. (6) and (7).

$$f_k(K_{ke} - K_e^*)\beta^k + f_{cl}(K_c^* - K_e^*)\beta^{cl} + f_m(K_{me} - K_e^*)\beta^m = 0$$
 (6)

$$f_{k}(\mu_{ke} - \mu_{e}^{*})\zeta^{k} + f_{cl}(\mu_{c}^{*} - \mu_{e}^{*})\zeta^{cl} + f_{m}(\mu_{me} - \mu_{e}^{*})\zeta^{m} = 0$$
 (7)

 $f_{\rm k},f_{\rm cl}$  and  $f_{\rm m}$  are the volume contents of organic matter, clay and matrix minerals, v/v, and  $f_{\rm k}+f_{\rm cl}+f_{\rm m}=$  1.  $K_{\rm e}^*$  and  $\mu_{\rm e}^*$  are the calculated equivalent bulk modulus and equivalent shear modulus, MPa

#### 3.2. Fusion of anisotropic PMs

According to SEM, there are many forms of clay and organic matter in shale. For layered clay and layered organic matter, this paper adopts the Backus average model to calculate the equivalent elastic modulus of layered clay and layered organic matter, and the calculation result can be equal to a laterally isotropic shale rock.

The average value of anisotropic Backus gives the transverse isotropic medium (VTI medium) described by five effective stiffnesses, and the equivalent medium elastic matrix expression is as follows (Backus, 1962):

$$A = C_{11} = C_{22} = \left\langle \frac{4\mu(\lambda + \mu)}{\lambda + 2\mu} \right\rangle + \left\langle \frac{1}{\lambda + 2\mu} \right\rangle^{-1} \left\langle \frac{\lambda}{\lambda + 2\mu} \right\rangle^{2} \tag{8}$$

$$C = C_{33} = \langle \frac{1}{\lambda + 2\mu} \rangle^{-1} \tag{9}$$

$$F = C_{13} = C_{31} = C_{32} = C_{23} = \left\langle \frac{1}{\lambda + 2u} \right\rangle^{-1} \left\langle \frac{\lambda}{\lambda + 2u} \right\rangle \tag{10}$$

$$D = C_{44} = C_{55} = \langle \frac{1}{\mu} \rangle^{-1} \tag{11}$$

$$M = C_{66} = \langle \mu \rangle \tag{12}$$

According to the established rock physics model, the weighted average of the physical quantity  $\alpha$  is defined as:

$$\langle \alpha \rangle = W_{\rm m} \alpha_{\rm m} + W_{\rm c} \alpha_{\rm c} + W_{\rm k} \alpha_{\rm k} \tag{13}$$

where, the subscripts c, k, and m respectively represent the mixture of layered clay minerals, layered organic matter, and all other compositions, and  $\lambda$  and  $\mu$  are the Lame coefficients of the medium. The parameter W is the average weight.

# 3.3. Equivalent medium models of shale with complex pore structure

There are many low-angle fractures in shale reservoirs, so the effect of fractures needs to be considered in the equivalent medium rock physics model. For anisotropic media, it is equivalent to adding the influence of fracture media based on the elastic parameter matrix  $\mathbf{C_b}$  of the background media. Based on the linear sliding model and the Hudson model, this paper constructs a fracture equivalent medium model, which conforms to the frequency and scale range of acoustic logging and can well simulate the propagation of waves in fractured media. The corresponding elastic matrix relationship is (Hudson, 1981):

where  $C_b$  is the elastic parameter matrix of the background medium,  $\Delta N$  is the tangential fracture strength, which reflects the fracture density,  $\Delta T$  is the normal fracture strength, which reflects the fluid filling degree in the fracture. And while the normal and tangential fracture strength increases, the ellipse flatness keeps increasing.

#### 3.4. The model validation

The model effect is verified by actual data of well X. Fig. 4 shows the depth from left to right, the first track is depth, and the second to sixth tracks are the volume of the matrix mineral (VMM), the volume of organic matter (VOM), the porosity of organic matter (POM), the volume of clay (VCL), and the porosity of clay (PCL). Among them, the VOM is calculated according to the density curve, the VCL is calculated according to the uranium curve, and the PCL and POM are calculated according to the "four pores" model (Li et al., 2014).

First, the isotropic model is used to simulate the acoustic time difference (DT), and the result is shown in the seventh track blue curve DTiso in Fig. 4 and is compared with the original measurement (the 7<sup>th</sup> red curve DT<sub>real</sub>). Although the general trends of the two lines are similar, the DTiso (blue line) obtained by the homogeneity model is quite different from the actual DT<sub>real</sub> (red). The modeled DT is generally small, and the result does not comply with the requirements of petrophysical modeling. Considering that the mineral composition contains layered clay and layered organic matter, adjusted the volume fraction of layered clay and layered organic matter, the DT simulated result of the equivalent medium model in this paper showing in Fig. 4 (the 8th track, blue curve, DT<sub>asi</sub>). For the convenience of comparison, the DT is simulated by the Backus model (the 8<sup>th</sup> green curve DT<sub>backus</sub>), and it can be found that DT<sub>asi</sub> coincides with the actual DT<sub>real</sub>, with good consistency. From the simulation results, it can be seen that the proposed shale reservoir model meets the actual requirements and has high reliability, which can be used to study the ALRL of the shale formation.

#### 4. Result and discussion

Using the PM established in this paper, the ALRL of shale is analyzed from two aspects of mineral composition and porosity, and the elastic parameters and density used in each part are shown in Table 1.

#### 4.1. Effect of compositions on acoustic log

Firstly, the ALRL of different mineral compositions (clay, organic matter, matrix minerals) is investigated. And in order to determine the response law of each component, the influence of porosity is not considered in the simulation.

Fig. 5 shows the response law of DT with clay content ( $V_{clay}$ ). The

rock model includes clay and matrix minerals (calcite, dolomite, quartz, and each account for one-third). Among them, clay is divided into layered clay and dispersed clay, and the layered clay content ( $V_{layerc}$ ) in clay ranges from 0 to 70%. It can be seen from Fig. 5 when the clay content is less than 20%, as the clay content increases, the compressive wave time difference (DTC, Fig. 5a) gradually decreases, and the layered clay has a small effect on the DTC and can be ignored: when clay volume content is more than 20% and layered clay content accounts for more than 50%, the DTC increases with the increase of clay volume content and the increasing rate increases with the increase of layered clay content. When the layered clay content is 70%, the growth rate is 2.2 times that of layered clay content being 50%. However, when the layered clay content is relatively small (less than 10%), the DTC decreases with the increase of clay volume content, and the decreasing amplitude increases with the decrease of layered clay. When the layered clay content is more than 50%, it has a minimum value when the clay content is 20%, and when the layered clay content is between 20% and 50%, it has a minimum value when the clay content is 30%, which indicates that layered clay has a greater influence on DTC than other forms of clay. And for the shear wave time difference (DTS, Fig. 5b), when the layered clay content is less than 10%, the DTS decreases with the increase of clay volume. When the content of layered clay is more than 10%, the DTS increases with the increase of clay volume content, and the increasing rate increases with the increase of layered clay content, which is 70%, and its increasing rate is 1.4 times that of layered clay with

Considering that the acoustic properties difference of matrix minerals (quartz, carbonate) are not obvious. This paper takes calcite as an example to study the influence of matrix mineral content on DT, and the rock model includes calcite and organic matter. Organic matter includes layered organic matter and dispersed organic matter. The proportion of layered organic matter ( $V_{\text{layk}}$ ) in organic matter ranges from 5% to 70%. Fig. 6 shows the response law of DT with calcite content. It can be seen from Fig. 6, DTC (Fig. 6a) and DTS (Fig. 6b) both decrease with the increase of calcite content ( $V_{\text{cal}}$ ), and when the content of calcite is the same, the DTC and DTS increase with the increase of layered organic matter content, while the layered organic matter content has little effect on the decreasing trend that the DTC and DTS with the increase of calcite content, and its decreasing rate is kept at 2.5  $\mu$ s/m per 0.1 unit volume (P-wave) and 70  $\mu$ s/m per 0.1 unit volume (S-wave)

Fig. 7 shows the response law of the DT with the organic matter content ( $V_{\text{kerogen}}$ ). At this time, the rock model includes organic matter and matrix minerals (calcite, dolomite, and quartz each account for one-third). Organic matter includes layered organic matter and dispersed organic matter, and layered organic matter accounts for 5%-70% of organic matter. It can be seen that the DT trends of compressive waves (Fig. 7a) and shear waves (Fig. 7b) are the same on the whole. And the DT (including compressive and shear waves) increases with the increase of organic matter content. When layered organic matter accounts for less than 50% of organic matter content, there is an approximately linear relationship between DT and organic matter content, and when layered organic matter accounts for more than 50%, DT and organic matter content are in the form of the approximate power function. At the same time, with the increase of layered organic matter content, the DT increases more obviously with the increase of organic matter; For P-wave, the growth rate of P-wave is 5 times as high as that of 5% when the layered organic matter content is 70%.

The research results show that the acoustic response law of clay minerals and organic matter is relatively complicated on the whole; while the DT response law of matrix minerals is relatively simple as

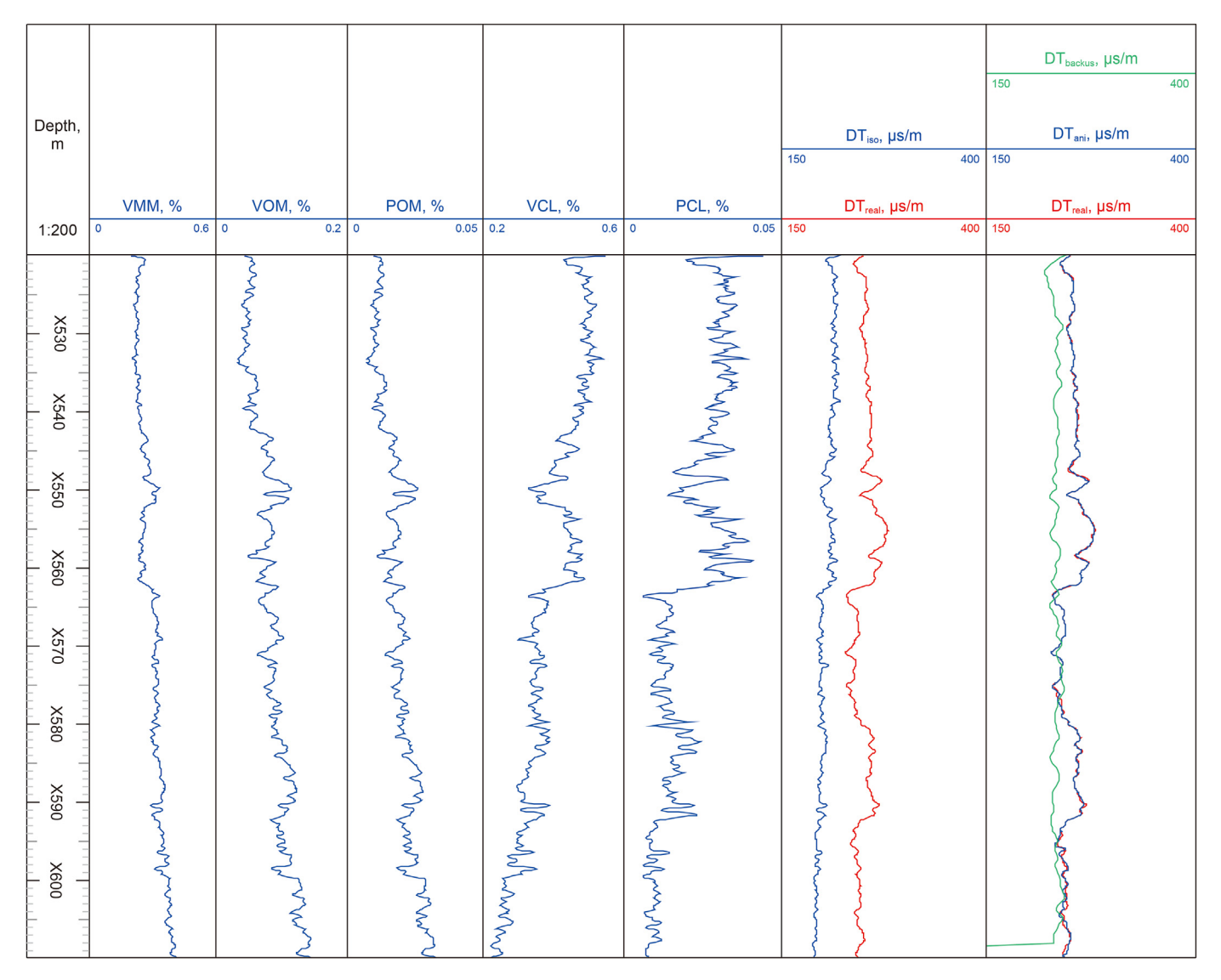


Fig. 4. Volume content of different components and petrophysical modeling results in well X.

**Table 1**Mineral composition and fluid parameters.

Composition	Bulk modulus, GPa	Shear modulus, GPa	Density, g/cm <sup>3</sup>
Clay	25	9	2.6
Quartz	37	44	2.65
Calcite	70.2	29	2.71
Dolomite	94.9	45	2.87
Organic matter	2.9	2.7	1.3
Water	2.23	0	1.04
Oil	0.86	0	0.79

a whole, and the DT has a linear relationship with the content of matrix minerals.

Fig. 8 shows the analysis of the influence of the DT and the anisotropy coefficient (define the anisotropic coefficient  $\varepsilon = \frac{V_{\rm ph}^2 - V_{\rm pv}^2}{2V_{\rm pv}^2}$ , where  $V_{\rm ph}$  and  $V_{\rm pv}$  are compressive wave velocity and shear wave velocity respectively, and the unit is m/s) on the volume content of layered clay. It can be seen that the compressive wave time difference (Fig. 8a) and the anisotropy coefficient (Fig. 8b) increase with the increase of the layered clay volume content

 $(V_{\rm layerc})$ . There is a linear relationship between DTC and layered clay content, and the lower the clay content, the more obvious the influence of layered clay, with an increased rate of 3/10 when the clay content is 60%. When the clay content  $(V_{\rm clay})$  is low, the volume content of layered clay has a significant influence on the anisotropy coefficient, and there is a linear relationship between them. When the content of layered clay is high, the volume content of layered clay has little influence on the anisotropy coefficient, and its growth rate is 1/20 of that of 10% when the content of layered clay is 60%.

### 4.2. Effect of pore types on acoustic log

According to the characteristics of shale pore structure, the forward modeling of organic pores, clay pores, clastic pores, and micro-fractures is carried out respectively, and their response rules to DT were summarized.

Fig. 9 shows the response law of DT with the change of organic matter pores. The rock model at this time includes organic matter and matrix minerals (calcite, dolomite, and quartz each account for one-third), and when it contains layered organic matter, the ratio of layered organic matter to organic matter is 10%. For the

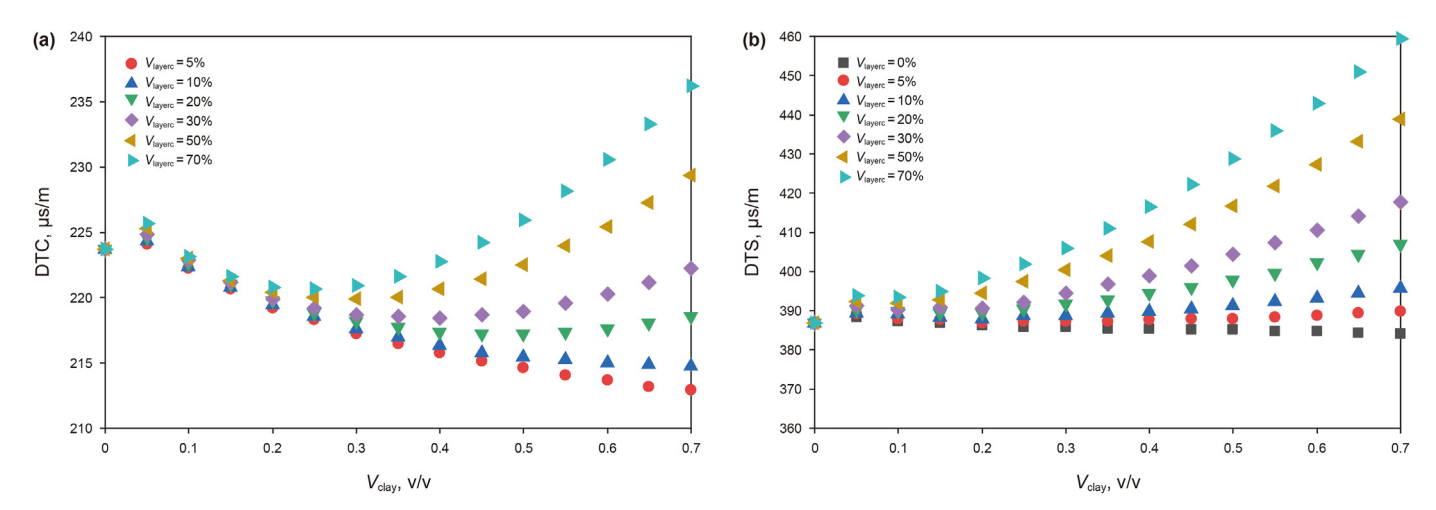


Fig. 5. The influence of clay volume content on acoustic properties.

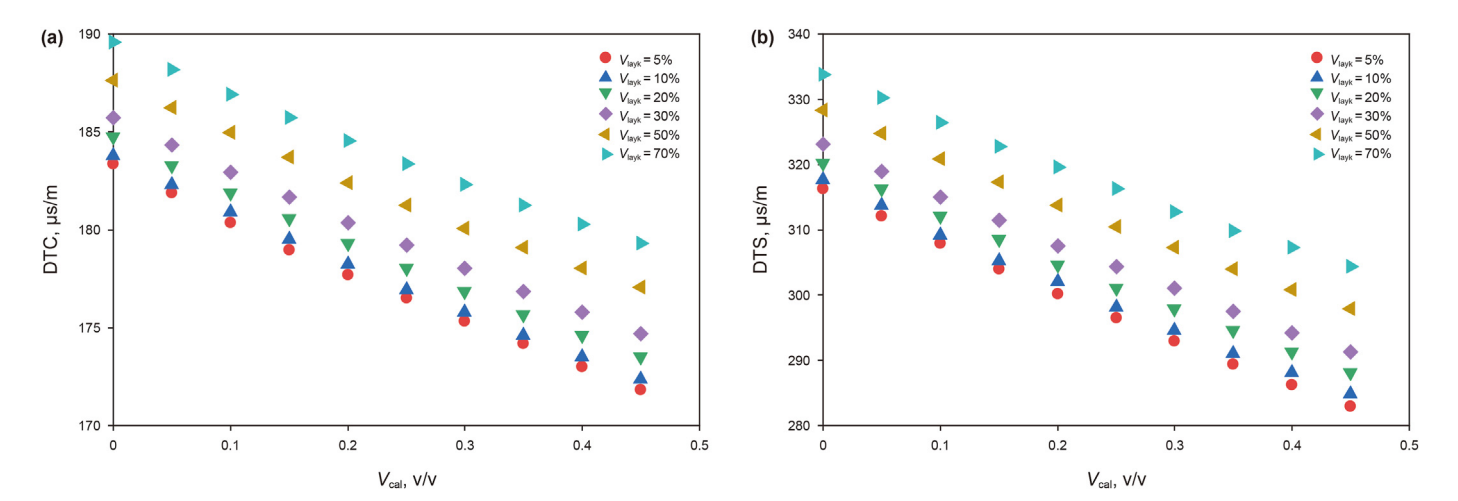


Fig. 6. The influence of calcite content on acoustic properties.

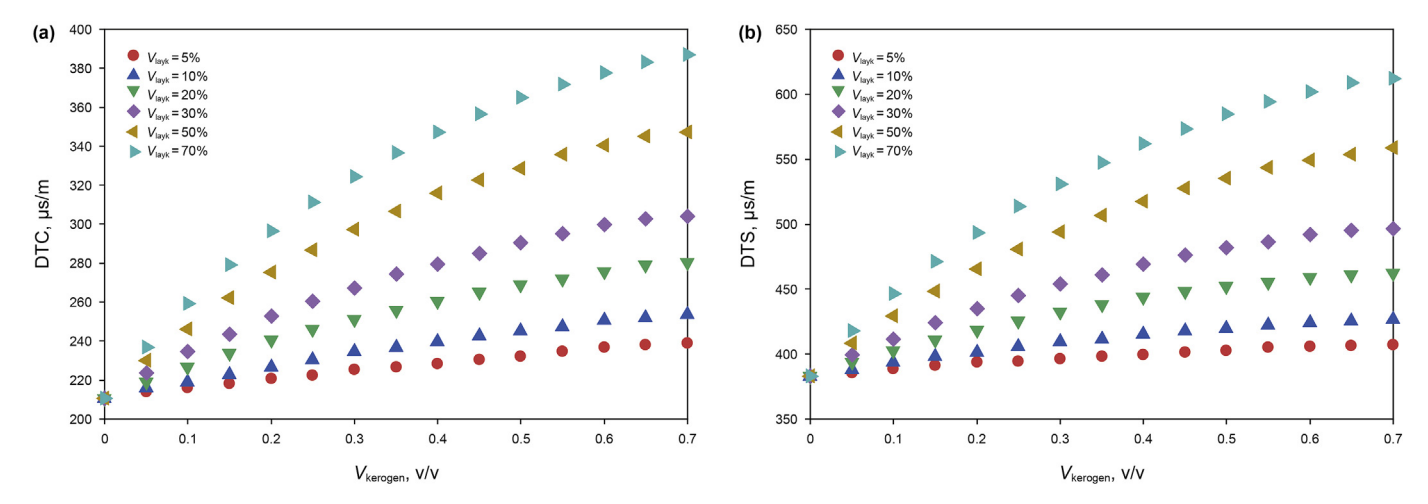


Fig. 7. The influence of organic matter content on acoustic properties.

compressive wave time difference (Fig. 9a), when it contains layered organic matter, DTC increases with the increase of the organic matter porosity, and when the organic matter content is low (< 45%), it changes linearly; but when the organic matter

content is high (> 45%), it shows an approximate exponential change law. For shear wave time difference (Fig. 9b), when the organic matter content is low, the change of organic matter porosity has little effect on the DTS; but when the organic matter

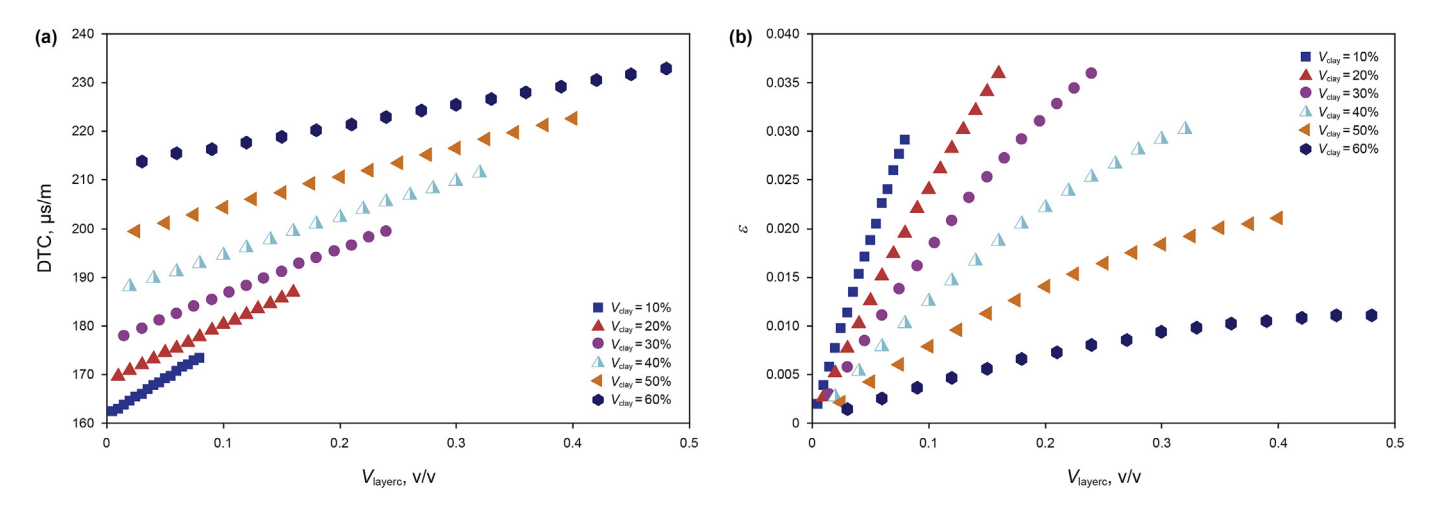


Fig. 8. The acoustic properties and anisotropy affected by volume content of layered clay.

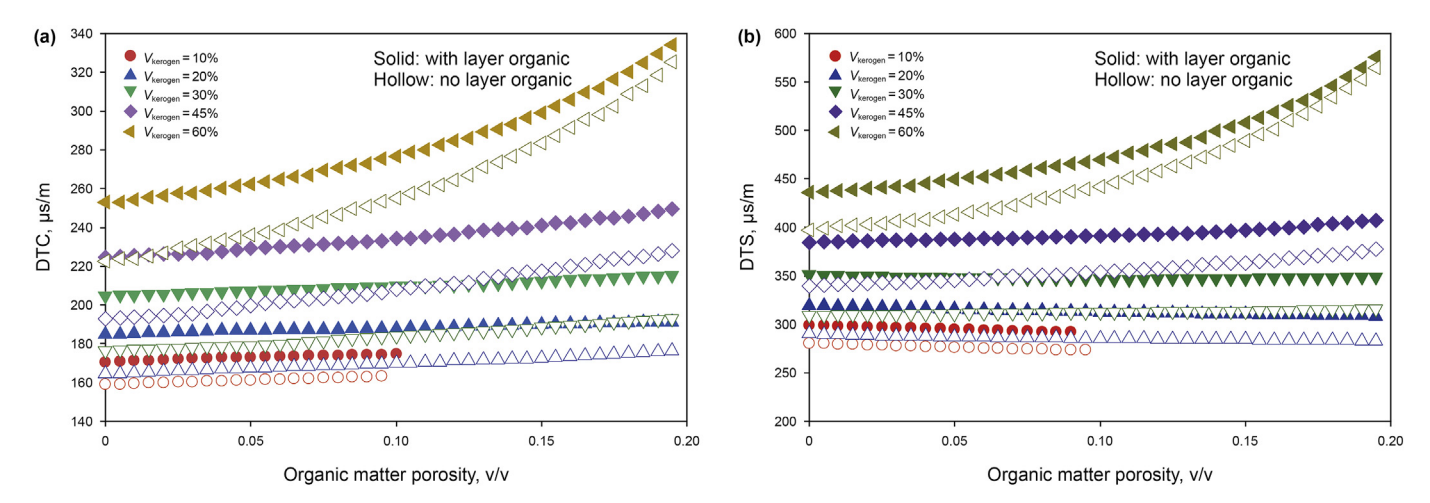


Fig. 9. The influence of organic matter porosity on acoustic properties.

content is high (> 45%), the DTS increases with the increase of organic matter porosity. When other conditions are the same, the changes of DT with organic porosity are consistent with those without layered organic matter. At the same time, without layered organic matter, the changing trend of time difference with organic porosity is more obvious, and its growth rate is 1.5 times that with layered organic matter. The difference is that the macroscopic anisotropy increases when layered organic matter is contained, and the DT is larger than that of rocks without layered organic matter.

Fig. 10 shows the response law of DT with the change of clay pores. And the rock model at this time includes organic matter and matrix minerals (calcite, dolomite, quartz, and each account for one-third); when there is layered clay, the layered clay accounts for 20% of the clay content.

It shows that the DTC increases with the increase of clay porosity, but when the clay content is low, the DTC increases linearly with the increase of clay porosity, and the DTS decreases slightly with the increase of clay porosity; but when the clay content is higher (> 45%), the DTS increases with the increase of clay porosity. When other conditions are the same, the change rule of DT with clay porosity is the same between layered clay and non-layered clay, and the changing trend of DT with clay porosity is more obvious without layered clay, and its growth rate is 1.3 times that of layered clay. The difference is that with layered clay, the

macroscopic anisotropy increases, and the DT is higher than that without layered organic matter.

Fig. 11 shows the response law of DT with the porosity of detrital minerals. The rock model at this time includes organic matter, clay, and matrix minerals (calcite, dolomite, quartz, and each account for one-third), in which clay and organic matter account for 20% of the total. It can be seen from the figure that the change law of DTC and DTS are relatively consistent, and both increase with the increase of clastic mineral porosity, showing an exponential function change trend. With the increase of organic matter content ( $V_{\rm kerogon}$ ), its growth rate also increases, and the growth rate under the condition of the organic matter content of 60% is 1.8 times that without organic matter.

The above analysis shows that the DT and porosities (clay porosity, clastic porosity, organic matter porosity) show a positive correlation on the whole, and only when the organic matter/clay content is low, the corresponding organic matter pores/clay pore change law is negative, and the influence of layered clay and layered organic matter on the response law is mainly reflected in anisotropy, and the DT increases under the same conditions.

#### 4.3. Effect of fracture on acoustic log

A large number of micro-fractures are developed in shale

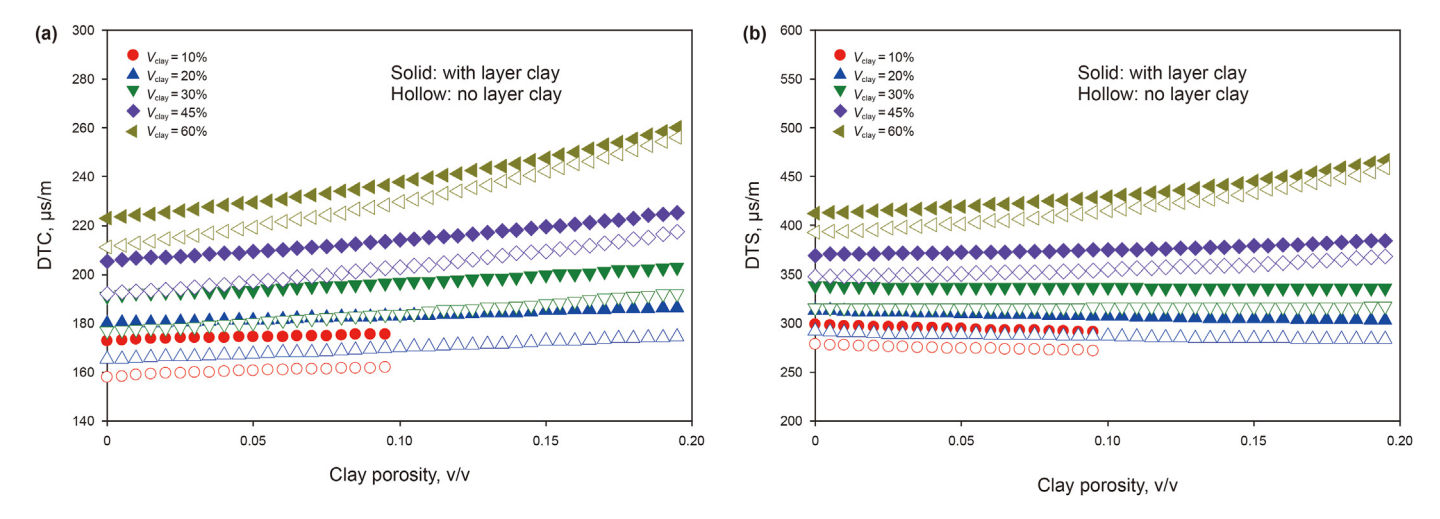


Fig. 10. The influence of clay pore on acoustic properties.

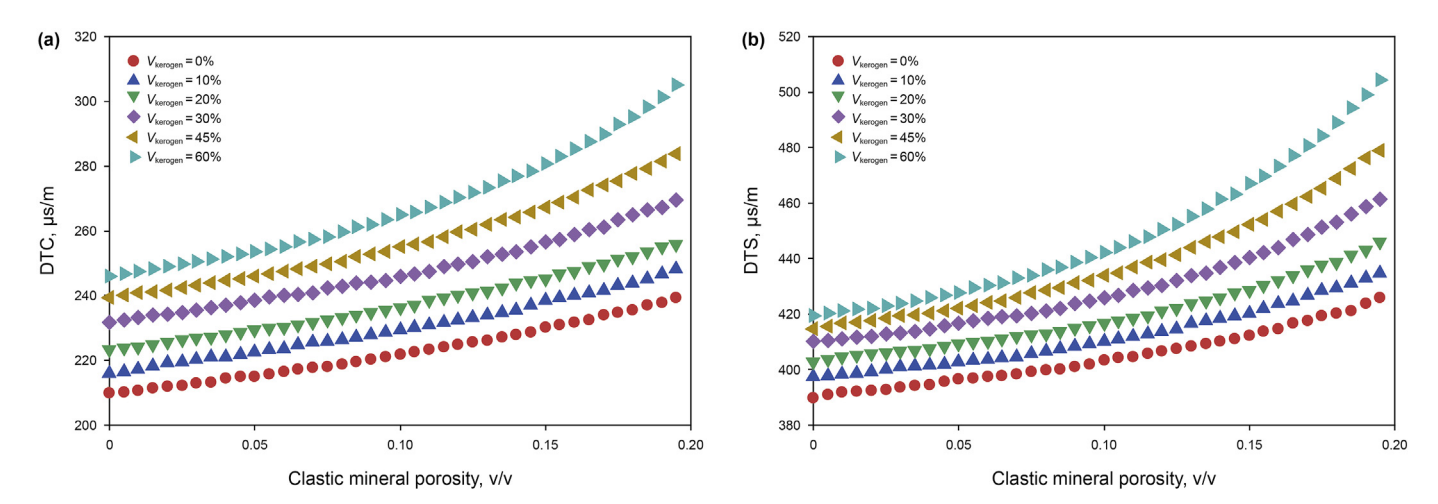
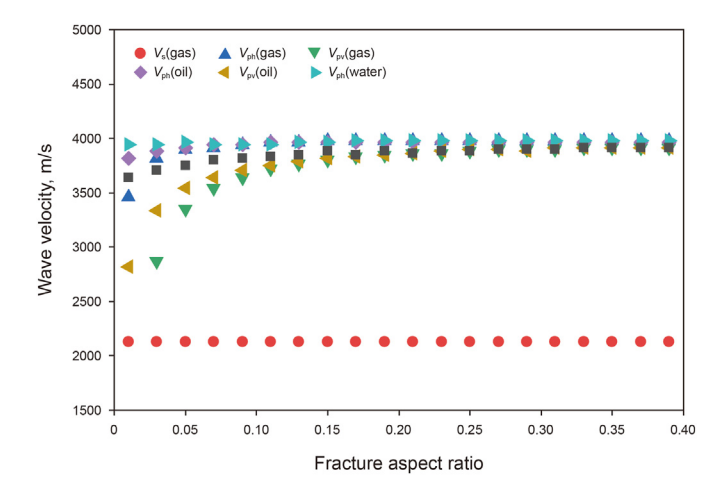


Fig. 11. The influence of clastic mineral pore on acoustic properties

reservoirs, and fracture porosity and fracture aspect ratio (ratio of fracture short axis length to fracture long axis length) is usually used as the main parameters of fracture description. This paper mainly simulates these two parameters to analyze the impact of fractures on wave velocity and time difference.

The simulated rocks include clay, matrix minerals, and organic matter (each accounting for one-third). When fracture porosity (Porf) is 1%, the relationship between the wave velocity and fracture aspect ratio under different fillings is simulated. In Fig. 12,  $V_{\rm p}$  is the compressive wave velocity,  $V_{\rm ph}$  and  $V_{\rm pv}$  represent the horizontal and vertical compressive wave velocity, and  $V_{\rm s}$  is the shear wave velocity. It can be seen from the figure that with the decrease of fracture aspect ratio, the  $V_{\rm s}$  remains unchanged, while the  $V_{\rm ph}$  and  $V_{\rm pv}$  decrease gradually, and the  $V_{\rm pv}$  decreases more obviously than the  $V_{\rm ph}$ , which is about 6.7 times as fast as  $V_{\rm ph}$ . At the same time, the velocity reduction rate of fracture to gas-bearing porous media is about 1.8 times that of oil-bearing porous media and about 5 times that of water-bearing porous media.

Fig. 13 shows the relationship between the anisotropy coefficient  $\varepsilon$  and the fracture aspect ratio when the fracture is filled with different fluid properties under different fracture porosity conditions. The Porf is the fracture porosity in this figure, varying from 0.3% to 1%, and the total porosity remains unchanged at 10%. Fig. 13 shows the fracture filled with water, oil, and gas respectively. It can



**Fig. 12.** The relationship between wave velocity and fracture aspect ratio under different fillers.

be seen that anisotropy decreases with the increase of fracture aspect ratio. For different fillers, the influence of fractures on anisotropy is also different. The anisotropy of gas-bearing fractures

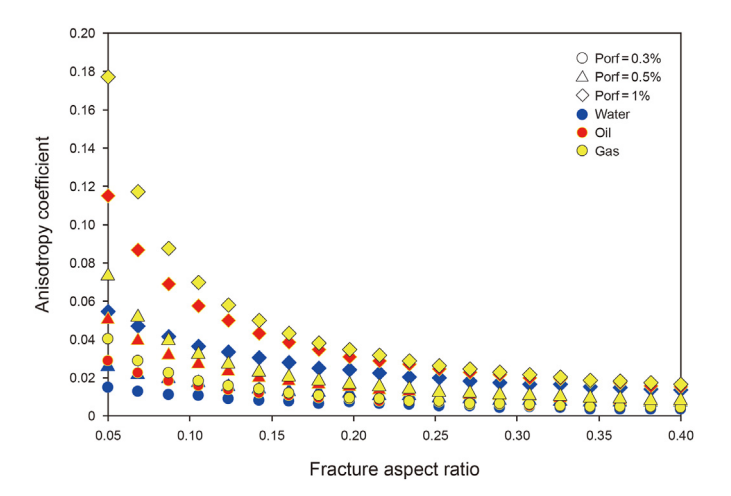


Fig. 13. Relationship between anisotropy and fracture aspect ratio under different fillers.

is 1.5 times that of oil-bearing fractures and 3.2 times that of waterbearing fractures, that is, the anisotropy degree of gas-bearing fractures > oil-bearing fractures > water-bearing fractures.

Fig. 14 shows the response law of acoustic velocity with fracture porosity when the fracture contains different fillings. It assumes that the aspect ratio of the fracture is 0.1. It can be seen that with the increase of fracture porosity, the P-wave velocity decreases gradually, and the wave velocity of gas-bearing porous media decreases 1.2 times as much as that of oil-bearing media and 1.8 times as much as that of water-bearing media. At the same time, the  $V_{\rm pv}$  decreases faster than the  $V_{\rm ph}$ , while the  $V_{\rm s}$  remains unchanged.

Fig. 15 shows the relationship between the anisotropy coefficient and the fracture porosity when the fracture is filled with different fluid properties under different total porosity (Port). It can be seen from the figure that when the fracture aspect ratio is constant, the greater the fracture porosity, the stronger the anisotropy of formation; and for different fillers, the influence of fractures on anisotropy is different; Under the total porosity is 5%, the anisotropy of gas-bearing fractures increases 1.5 times as fast as that of oil-bearing fractures and 3.3 times as fast as that of water-bearing, that is, the anisotropy degree of gas-bearing fractures > that of oil-bearing fractures > that of water-bearing fractures. By comparing and analyzing the anisotropy laws of

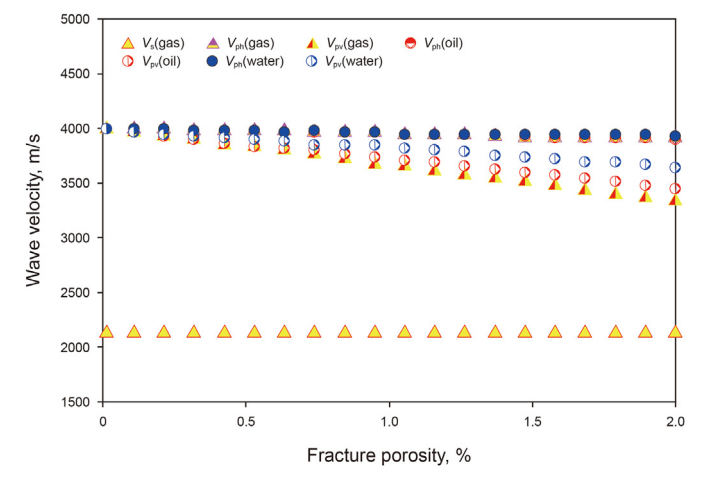


Fig. 14. The relationship between wave velocity and fracture porosity in different fillers.

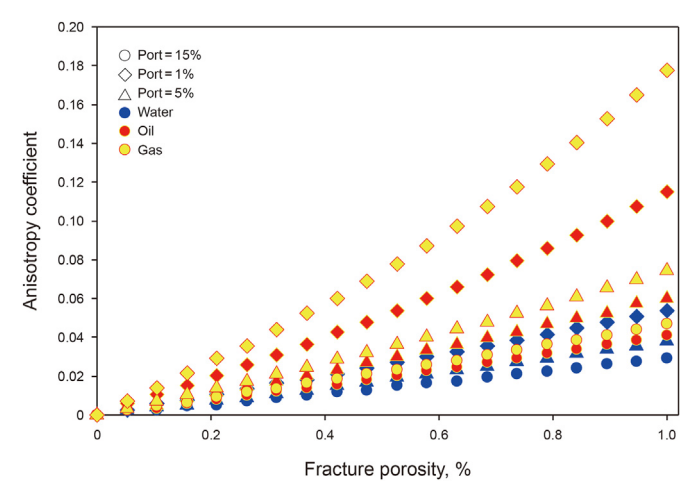


Fig. 15. The correlation between anisotropy coefficient and fracture porosity under different fillers.

layered clay and micro-fractures, there is an order of magnitude difference between them, and fractures are the main controlling factors of shale anisotropy.

#### 5. Conclusion

- (1) We usd the Kuster-Toksöz model, SCA model, Voigt model, Backus model and Hudson model to establishe a shale rock physics model with complex pores. The actual logging data show that the model is reasonable and effective for acoustic prediction of shale formation with complex pore structure and small pore size.
- (2) When the clay content is less than 20%, the DTC decreases with the increase of clay content, otherwise the DTC increases with the increase of clay volume content. DTC and DTS decrease with the increase of calcite content and increase with the increase of organic matter content.
- (3) The DTC and DTS increase with the increase of organic porosity and clay porosity. The changing trend of DT with clay/organic porosity is more obvious without layered, and its growth rate is 1.5 times that of layered organic matter, and is 1.3 times that with layered clay. The clastic porosity increases with the DTC and DTS, showing an exponential function change trend.
- (4) When the fracture aspect ratio is constant, the anisotropy degree of formation is stronger with the increase of fracture porosity, and the anisotropy degree of gas-bearing fracture > oil-bearing fracture > water-bearing fracture. The influence of fracture on anisotropy is greater than that of clay, which is the main controlling factor of shale anisotropy

#### Acknowledgement

This work was financially supported by the National Natural Science Foundation of China (NSFC) Basic Research Program on Deep Petroleum Resource Accumulation and Key Engineering Technologies (Grant No. U19B6003-04-03-03), The Key Project of Sinopec Ministry of Science and Technology (Grant No.PE19012-1), and the National Research Council of Science and Technology Major Project (Grant No. 2016ZX05060-001-012).

#### References

Aleardi, M., 2018. Applying a probabilistic seismic-petrophysical inversion and two

different rock-physics models for reservoir characterization in offshore Nile Delta. J. Appl. Geophys. 148, 272–286. https://doi.org/10.1016/j.jappgeo.2017.12.006.

- Backus, G.E., 1962. Long-wave elastic anisotropy produced by horizontal layering. J. Geophys. Res. 67 (11), 4427–4440. https://doi.org/10.1029/JZ067i011p04427.
- Berryman, J.G., 1995. Mixture theories for rock properties. Rock physics and phase relations: A handbook of physical constants 3, 205–228.
- Chen, S., Han, Y., Fu, C., et al., 2016. Micro and nano-size pores of clay minerals in shale reservoirs: implication for the accumulation of shale gas. Sediment. Geol. 342, 180–190. https://doi.org/10.1016/j.sedgeo.2016.06.022.
- Cleary, M.P., Chen, I.W., Lee, S.M., 1980. Self-consistent techniques for heterogeneous media. J. Eng. Mech. 106 (5), 861–887. https://doi.org/10.1061/ IMCEA3.0002740.
- Coates, R.T., Schoenberg, M., 1995. Finite-difference modeling of faults and fractures. Geophysics. 60 (5), 1514–1526. https://doi.org/10.1190/1.1443884.
- Ding, P.B., Gong, F., Zhang, F., et al., 2021. A physical model study of shale seismic responses and anisotropic inversion. Petrol. Sci. 18 (4), 1059–1068. https:// doi.org/10.1016/j.petsci.2021.01.001.
- Gassmann, F., 1951. Elastic waves through a packing of spheres. Geophysics. 16 (4), 673–685. https://doi.org/10.1190/1.1437718.
- Guo, Z., Li, X., Liu, C., et al., 2013. A shale rock physics model for analysis of brittleness index, mineralogy and porosity in the Barnett Shale. J. Geophys. Eng. 10 (2), 25006. https://doi.org/10.1007/s12182-021-00555-0.
- He, Y.X., Li, X.L., Tang, G.Y., et al., 2021. Modeling the effects of fracture in fill on frequency-dependent anisotropy and AVO response of a fractured porous layer. Petrol. Sci. 18, 758–772. http://iopscience.iop.org/1742-2140/10/2/025006.
- Hill, R., 1952. The elastic behavior of crystalline aggregate. Proc. Phys. Soc. A65 (5), 349–354.
- Hornby, B.E., Schwartzt, L.M., Hudson, J.A., 1994. Anisotropic effective-medium modeling of the elastic properties of shales. Geophysics. 59 (10), 1570–1583. https://doi.org/10.1016/0148-9062(95)93233-F.
- Hu, Q., Chen, X.H., Li, J.Y., 2014. Shear wave velocity prediction for shale gas reservoirs based on anisotropic rock physics model. Geophys. Prospect. Pet. 53 (3), 254–261. https://doi.org/10.3969/j.issn.1000-1441.2014.03.002 (in Chinese).
- Hudson, J.A., 1981. Wave speeds and attenuation of elastic waves in material containing cracks. Geophys. J. Roy. Astron. Soc. 64 (1), 133–150. https://doi.org/10.1111/j.1365-246X.1981.tb02662.x.
- Jin, Z.J., Hu, Z.Q., Gao, B., et al., 2016. Controlling factors on the enrichment and high

- productivity of shale gas in the Wufeng-Longmaxi Formations, southeastern Sichuan Basin. Earth Sci. Front. 23 (1), 1–10. https://doi.org/10.13745/j.esf.2016.01.001 (in Chinese).
- Kuster, G.T., Toksoz, M.N., 1974. Velocity and attentation of seismic waves in two phase media: Part 1, Theoretical formulation. Geophysics. 39 (5), 587–606. https://doi.org/10.1190/1.1440450.
- Li, J., Lu, J., Li, Z., et al., 2014. 'Four-pore' modeling and its quantitative logging description of shale gas reservoir. Oil Gas Geol. 35 (2), 266–271. https://doi.org/10.11743/ogg20140214 (in Chinese).
- Mavko, G., Mukerji, T., Dvorkin, J., 2020. The Rock Physics Handbook. Cambridge university press.
- Qian, C., Yang, S.C., Wang, Y., et al., 2021. Prediction and modeling of petrophysical parameters of deep-buried, low permeability glutenite reservoirs in Yubei area, Turpan-Hami Basin, China. J. Petrol. Sci. Eng. 207, 109154. https://doi.org/10.1016/j.petrol.2021.109154.
- Shen, B.J., Yang, Y.F., Ten, G.E., et al., 2016. Characteristics and hydrocarbon significance of organic matter in shale from the Jiaoshiba structure, Sichuan Basin: a case study of the Wufeng-Longmaxi formations in well Jiaoye1. Pet. Geol. Exp. 38 (4). https://doi.org/10.11781/sysydz201604480, 480-488+495(in Chinese).
- Vernik, L., Milovac, J., 2011. Rock Physics of organic shales. Lead. Edge. 30 (3), 318–323. https://doi.org/10.1190/1.3567263.
- Wang, Z.G., 2015. Breakthrough of Fuling shale gas exploration and development and its inspiration. Oil Gas Geol. 36 (1), 1–6. https://doi.org/10.11743/ogg20150101 (in Chinese).
- Wang, T., Zhao, H.B., Li, K.Z., et al., 2019. A mud shale seismic rock physics model considering complex pore structure. J. Univ. Pet., China (Ed. Nat. Sci.). 43 (3), 45–55. https://doi.org/10.3969/j.issn.1673-5005.2019.03.005 (in Chinese).
- Wu, W.T., Grana, D., 2017. Integrated petrophysics and rock physics modeling for well log interpretation of elastic, electrical, and petrophysical properties. J. Appl. Geophys. 146, 54–66. https://doi.org/10.1016/j.jappgeo.2017.09.007.
- Wu, T., Liu, X.J., Yuan, W., et al., 2016. Acoustic characteristics of longmaxi shale in southeast sichuan. West-China Explor. Eng. 28 (2), 72–75. https://doi.org/ 10.3969/j.issn.1004-5716.2016.02.024 (in Chinese).
- Zhao, J.H., Jin, Z.K., Jin, Z.J., et al., 2017. Origin of authigenic quartz in organic-rich shales of the Wufeng and longmaxi formations in the Sichuan Basin, south China: implications for pore evolution. J. Nat. Gas Sci. Eng. 38, 21–38. https://doi.org/10.1016/j.jngse.2016.11.037.